

GALAXIES IN X-RAY GROUPS. III. SATELLITE COLOR AND MORPHOLOGY TRANSFORMATIONS

MATTHEW R. GEORGE^{1,2}, CHUNG-PEI MA¹, KEVIN BUNDY³, ALEXIE LEAUTHAUD³, JEREMY TINKER⁴, RISA H. WECHSLER^{5,6}, ALEXIS FINOGUENOV⁷, BENEDETTA VULCANI³

Draft version August 28, 2018

ABSTRACT

While the star formation rates and morphologies of galaxies have long been known to correlate with their local environment, the process by which these correlations are generated is not well understood. Galaxy groups are thought to play an important role in shaping the physical properties of galaxies before entering massive clusters at low redshift, and transformations of satellite galaxies likely dominate the buildup of local environmental correlations. To illuminate the physical processes that shape galaxy evolution in dense environments, we study a sample of 116 X-ray selected galaxy groups at $z = 0.2 - 1$ with halo masses of $10^{13} - 10^{14} M_{\odot}$ and centroids determined with weak lensing. We analyze morphologies based on *HST* imaging and colors determined from 31 photometric bands for a stellar mass-limited population of 923 satellite galaxies and a comparison sample of 16644 field galaxies. Controlling for variations in stellar mass across environments, we find significant trends in the colors and morphologies of satellite galaxies with group-centric distance and across cosmic time. Specifically at low stellar mass ($\log(M_{\star}/M_{\odot}) = 9.8 - 10.3$), the fraction of disk-dominated star-forming galaxies declines from $> 50\%$ among field galaxies to $< 20\%$ among satellites near the centers of groups. This decline is accompanied by a rise in quenched galaxies with intermediate bulge+disk morphologies, and only a weak increase in red bulge-dominated systems. These results show that both color and morphology are influenced by a galaxy's location within a group halo. We suggest that strangulation and disk fading alone are insufficient to explain the observed morphological dependence on environment, and that galaxy mergers or close tidal encounters must play a role in building up the population of quenched galaxies with bulges seen in dense environments at low redshift.

Subject headings: galaxies: bulges – galaxies: clusters: general – galaxies: evolution – galaxies: halos – galaxies: statistics – X-rays: galaxies: clusters

1. INTRODUCTION

Galaxy properties are correlated with their environment. Dense regions host galaxies with greater masses, lower star-formation rates, and morphologies that are more bulge-dominated than in low density regions. Since the early work of Dressler (1980), studies of environmental correlations have expanded to a variety of indicators of star formation, morphology, and environment. See Blanton & Moustakas (2009) for a recent review of these correlations in the local universe.

Numerous processes may be culpable for the dependence of galaxy properties on environment (see Boselli & Gavazzi 2006 for a review). Galaxy interactions through mergers or tides can disrupt stellar kinematics and remove gas. These interactions can also apply torques that

drive gas inward, perhaps feeding star formation or a central black hole. Halos can play a role through tidal forces and dynamical friction. Pressure from hot dense gas inside halos may strip gas from infalling galaxies, and shock heating in massive halos can prevent accretion of cold gas that would feed star formation.

Despite extensive observational and theoretical work, the dominant physical mechanisms responsible for the environmental correlations remain unclear. An important clue is that the scale on which these correlations appear is similar to the size of the dark matter halos hosting galaxies (e.g., Kauffmann et al. 2004; Blanton & Berlind 2007). Relatedly, satellite galaxies have a primary role in the buildup of the red sequence in dense environments (e.g., Weinmann et al. 2006; van den Bosch et al. 2008; Wetzel et al. 2012a; Peng et al. 2012).

Since many galaxy characteristics are interrelated, it is important to study the correlations for each property independently while fixing other variables. When constraining environmental effects, one ideally controls for differences in redshift, stellar mass, halo mass, and location within a group. The colors and morphologies of galaxies are also correlated, so it is advantageous to split galaxies simultaneously by color and morphological classes to distinguish between processes that affect star formation rates and structural properties differently. Several studies have suggested that environmental processes affect star formation more significantly than morphology (e.g., Kauffmann et al. 2004; Blanton et al. 2005; Christlein & Zabludoff 2005; Weinmann et al. 2009; Kovač et al. 2010), suggesting that the gas that feeds star

mgeorge@astro.berkeley.edu

¹ Department of Astronomy, University of California, Berkeley, CA 94720, USA

² Lawrence Berkeley National Laboratory, 1 Cyclotron Road, Berkeley, CA 94720, USA

³ Kavli Institute for the Physics and Mathematics of the Universe (Kavli IPMU, WPI), Todai Institutes for Advanced Study, University of Tokyo, Kashiwa 277-8583, Japan

⁴ Center for Cosmology and Particle Physics, Department of Physics, New York University, 4 Washington Place, New York, NY 10003, USA

⁵ Kavli Institute for Particle Astrophysics and Cosmology, SLAC National Accelerator Laboratory, 2575 Sand Hill Rd., Menlo Park, CA 94025, USA

⁶ Physics Department, Stanford University, Stanford, CA 94305, USA

⁷ Department of Physics, University of Helsinki, Gustaf Hällströmin katu 2a, FI-00014 Helsinki, Finland

formation is depleted or removed without significantly altering galactic structure or stellar kinematics.

While many of the observational studies have focused on large surveys at low redshift or on massive clusters at higher redshifts, less is known about the more common group-scale environments and their evolution over time. In this paper, we study the colors and morphologies of galaxies in groups spanning the redshift range $z = 0.2 - 1$. We focus in particular on the properties of satellite galaxies as a function of stellar mass, group-centric distance, and redshift. This sample of groups has been identified from the COSMOS field (Scoville et al. 2007) based on their extended X-ray emission and have masses determined with weak lensing in the range $10^{13} - 10^{14} M_{\odot}$ (Leauthaud et al. 2010). Galaxy membership has been assigned using precise photometric redshifts with a Bayesian procedure tested extensively with mock catalogs and a spectroscopic subsample (George et al. 2011). Furthermore, by finding galaxies that maximize the lensing signal on small scales we have identified central galaxies that accurately trace the center of mass of their halos (George et al. 2012). Additional studies of these groups with magnification lensing (Ford et al. 2012; Schmidt et al. 2012) and clustering (Allevato et al. 2012) have confirmed the halo mass estimates. These ingredients make for a robust characterization of group environments with which to study satellite properties and their evolution over time.

We describe the data used in this analysis in Section 2 along with mock catalogs used to estimate the purity of the satellite population analyzed. Section 3 presents the results including our primary finding of a declining fraction of blue late disk galaxies and a rise in red early types toward group centers and over cosmic time. In Section 4, we discuss the implications of these findings for the physical mechanisms that shape galaxy evolution, and put this work in the context of previous studies and possibilities for the future.

2. DATA AND MOCKS

The COSMOS field (Scoville et al. 2007) has been the subject of a broad array of multi-wavelength imaging and spectroscopy campaigns. In this study we make use of several pieces of this data: galaxy colors, photometric redshifts, and stellar masses derived from over thirty bands of ultraviolet, optical, and infrared data (Ilbert et al. 2009, 2010; Bundy et al. 2010); galaxy morphologies determined by Scarlata et al. (2007) from high-resolution imaging taken by the Advanced Camera for Surveys (ACS) aboard the *Hubble Space Telescope* (Koekemoer et al. 2007); and a catalog of massive galaxy groups selected based on their X-ray emission seen with *XMM-Newton* and *Chandra* and for which halo mass profiles have been characterized using weak lensing with *Hubble* imaging (Leauthaud et al. 2010; George et al. 2011, 2012). Most of these data have been compiled in the group member catalog published in George et al. (2011) and we refer the reader to that paper and references therein for further details including the flux and mass limits for galaxies and groups. Here we briefly explain the stellar masses, colors, and morphologies used in this paper, as well as the identification of group centers and the mock catalogs used for validating group membership assignment and estimating the effects of contamination

from field galaxies.

2.1. Group Membership and Mocks

As a measure of galaxy environment, we use a catalog of groups described in George et al. (2011). These groups have been identified through a wavelet detection of extended X-ray emission following Finoguenov et al. (2010) and the sample is an expanded version of an earlier COSMOS catalog (Finoguenov et al. 2007) with deeper X-ray data. A Bayesian membership algorithm is used to associate galaxies with groups based on precise photometric redshifts and proximity to the X-ray position, with a prior accounting for the relative field population as a function of magnitude and redshift. Following George et al. (2011), we select galaxies with membership probability $P_{\text{mem}} > 0.5$ among the clean sample of groups, avoiding masked regions, groups with fewer than four members, overlapping groups, and possible projections (FLAG_INCLUDE=1 in the catalog). Halo masses for these groups have been measured with stacked weak lensing to be in the range $M_{200c} \approx 10^{13} - 10^{14} M_{\odot}$ and are correlated with X-ray luminosity (Leauthaud et al. 2010; George et al. 2012). Over this limited range in halo masses, we have not detected significant trends in galaxy properties with X-ray luminosity, but to avoid the influence of outliers we eliminate a small number of groups with halo masses estimated from their X-ray luminosities following Leauthaud et al. (2010) that are above or below the $10^{13} - 10^{14} M_{\odot}$ range.

We split galaxies into central, satellite, and field populations across several stellar mass and redshift bins to isolate dependences among different properties. For each group, the central galaxy is defined as the most massive group member within a projected distance of the X-ray position equal to the scale radius of a Navarro-Frenk-White (Navarro et al. 1996) profile. George et al. (2012) showed with weak lensing tests that this definition traces the halo center to within roughly 75 kpc, though in roughly 30% of groups the center is still ambiguous. In this paper we do not specifically study the central galaxies in these X-ray selected halos because their abundance limits statistical constraints on the properties of this population. The remaining group members are called satellites, and are the primary focus of this work. Field galaxies are taken to be those not assigned to any extended X-ray source and are thus expected to reside in halos less massive than the X-ray detection limit ($P_{\text{mem}} = 0$ from George et al. 2011; see Figure 1 of that paper for the X-ray flux limit as a function of redshift). Because we do not detect faint X-ray groups at high redshift, the halo mass range occupied by the field population can evolve due to this selection effect. However, at low redshift only $\sim 10\%$ of galaxies in our sample live in X-ray groups, so we expect the evolving halo mass limit to have only a small effect on the statistics of the field population. Table 1 gives the size of each of these samples used in our analysis.

Extensive tests of the accuracy of the photometric redshifts and membership assignment algorithm have been carried out using mock catalogs from simulations as well as a subsample of galaxies with spectroscopic redshifts (George et al. 2011). The overall purity and completeness of the member selection within $0.5R_{200c}$ is 84% and 92%, respectively, down to our flux limit of $F814W = 24.2$.

TABLE 1
ENVIRONMENTAL CENSUS

Type	Stellar Mass [$\log(M_*/M_\odot)$]	
	[9.8, 10.3)	[10.3, 10.8)
$z = 0.2 - 0.5; N_{\text{groups}} = 47$		
Satellites	237	218
Field	2455	1993
$z = 0.5 - 0.8; N_{\text{groups}} = 40$		
Satellites	122	189
Field	4497	3529
$z = 0.8 - 1.0; N_{\text{groups}} = 29$		
Satellites	...	157
Field	...	4170

NOTE. — No contamination corrections have been applied. Ellipses denote a bin below our stellar mass completeness limit.

The accuracy of member selection depends most significantly on distance from the group center and on the flux of a galaxy. The first effect is due to the decreasing density of true members with group-centric distance, which implies that selecting galaxies uniformly with radius (out to R_{200c}) will result in higher contamination from field galaxies in the outskirts. The second effect from galaxy flux arises from the decreasing precision of photometric redshifts for fainter galaxies, ranging from $\sigma_z \lesssim 0.01$ at $F814W < 22.5$ to $\sigma_z = 0.03$ at $F814W = 24$. It is notable that with the many filters used in constructing these photometric redshifts, precision does not depend significantly on spectral type, so red and blue galaxies of a given magnitude are selected with similar completeness.

In our analyses of member populations, we correct for contamination from field galaxies using the mock catalogs described in George et al. (2011). A halo catalog is constructed from a LasDamas simulation (C. K. McBride et al., in preparation)⁸ and populated with group members following the halo occupation model of Leauthaud et al. (2012). Mock galaxies are matched to real COSMOS galaxies in narrow bins of stellar mass and redshift to assign magnitudes in the F814W band, which in turn are used to assign mock photometric redshift errors. We estimate the purity of the member selection algorithm in bins of group-centric distance and magnitude, and assume that the colors and morphologies of contaminating field galaxies are representative of the field population at that magnitude. Contamination corrections are applied to the satellite populations only, since the field population is much larger. These corrections only account for contamination of the member list and not for incompleteness; the latter effect is smaller, does not significantly depend on group-centric distance, and should be fairly uniform across galaxy types since the precision of photometric redshifts is effectively achromatic (see Figures 2 and 5 of George et al. 2011).

2.2. Stellar Masses, Colors, and Morphologies

⁸ Details regarding the LasDamas ‘‘Consuelo’’ simulation can be found at <http://lss.phy.vanderbilt.edu/lasdamas/simulations.html>

Stellar masses and spectral classes have been determined by fitting stellar population synthesis models to the spectral energy distributions of galaxies, varying the age, amount of dust extinction, and metallicity in the models. We use the stellar masses from Bundy et al. (2010) and color classifications from Ilbert et al. (2010), both of which are based on Bruzual & Charlot (2003) models fit with a Chabrier (2003) initial mass function but take somewhat different approaches to fitting the data. Using the unextincted rest-frame color ($\text{NUV} - r^+$) of the best-fitting template for each galaxy, we split them into two color classes:

- *red*: $(\text{NUV} - r^+) > 3.5$
- *blue*: $(\text{NUV} - r^+) < 3.5$.

Ilbert et al. (2010) showed that this color cut corresponds with a specific star formation rate of roughly 10^{-11}yr^{-1} . It is worth emphasizing that these colors are corrected for dust extinction, so that the red sample selects a population of quiescent galaxies similar to those identified using two color cuts based on near-ultraviolet, optical, and near-infrared measurements, minimizing contamination from dusty star-forming galaxies (e.g., Bundy et al. 2010).

Galaxies are classified morphologically based on automated measurements of several structural parameters from ACS imaging in the F814W band. We use the Zurich Estimator of Structural Types (ZEST; Scarlata et al. 2007) catalog, which is derived from measurements of the asymmetry, concentration, Gini coefficient, second moment of the brightest pixels, and ellipticity. Scarlata et al. (2007) performed a principal component analysis of these measured quantities to identify the most important structural parameters, and divided galaxies into classes (early type, disk, and irregular) based on their location in this principal component space. A further subdivision of the disk category was derived by correlating measurements of the Sérsic index for a bright sample with $I_{AB} < 22.5$ with location in the principal component space. This parametrization provides a rough indication of the bulge-to-disk ratio, with four classes ranging from bulge-dominated to bulgeless disks. For statistical purposes, we consolidate some of these classifications into three morphological categories:

- early type *spheroidals* and bulge-dominated disks including even relatively inclined S0 galaxies (ZEST types 1 and 2.0)
- intermediate *bulge+disk* galaxies (ZEST type 2.1)
- *late disks* with little or no bulge component (ZEST types 2.2 and 2.3).

Irregulars and unclassified galaxies make up a small fraction of the sample, typically not more than a few percent in any stellar mass bin. We note that morphological K-corrections, which have not been applied, should not have a large effect on our sample because the F814W band probes rest-frame optical wavelengths over our entire redshift range (e.g., Lotz et al. 2004; Cassata et al. 2005; Bundy et al. 2010).

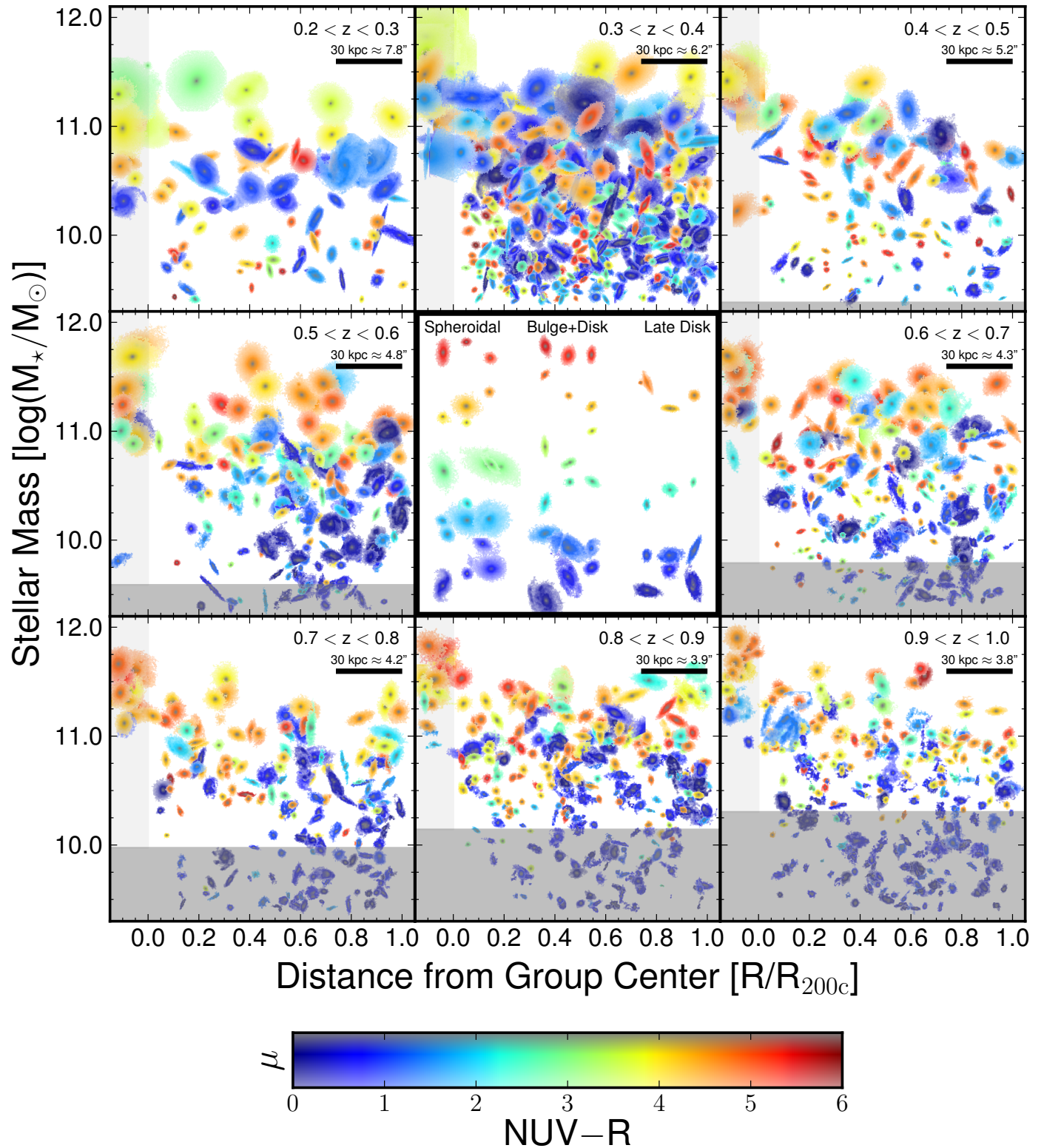


FIG. 1.— Group members as a function of stellar mass and distance from the group center. Colors for each galaxy represent the average unextinguished rest-frame template ($\text{NUV} - r^+$) color, with shading proportional to the logarithmic surface brightness μ . The gray band at the bottom of the high-redshift panels shows the stellar mass completeness limit for a passive population calculated with our flux limits $F_{814W} = 24.2$ and $K_s = 24$ following the approach of Bundy et al. (2010) (see also Figure 1 of George et al. 2011). Central galaxies in these groups are shown in the light gray band on the left side of each of the outer panels. The middle frame shows morphological classifications for a random sample of galaxies chosen to span the range of colors observed; objects in this panel are sorted vertically by color and horizontal offsets within each classification are arbitrary.

3. RESULTS

We begin our analysis with a visualization of a few properties of the galaxies in our sample. Figure 1 shows the distributions of stellar masses and group-centric distances in different redshift bins for all galaxies selected as group members. Each point represents one object and is displayed using the ACS image of the galaxy (Koekemoer et al. 2007), colored according to the average unextincted rest-frame template ($\text{NUV} - r^+$) color. Centrals are positioned on the left of each panel with small horizontal offsets, and satellites are plotted at their distance from the corresponding central. Each image is basically the set of adjacent pixels with flux above a noise threshold shown with a logarithmic surface brightness scale that has its maximum set to the peak value for each galaxy. We note that the apparent size of a galaxy on the plot is quite sensitive to its flux since images of brighter galaxies have more pixels above the noise threshold, and this is not a perfect indicator of the physical effective radius of a galaxy. A small fraction of objects have deblending issues or edge effects from the cutout image size, but we note that the images are processed independently for visualization and analysis purposes.

Several trends are evident when visualizing galaxies in this manner. Stellar mass is a strong determinant of galaxy properties; massive galaxies are more likely to be large, red, and spheroidal. Physical properties also depend on the location within a group. Central galaxies are massive (by definition), but also typically red and elliptical. Blue centrals tend to be less massive than red centrals at high redshifts even within the fairly narrow range of halo masses studied here, as discovered by Tinker et al. (2012). Satellites closer to group centers are more likely to be red and show fewer spiral features than in the outskirts, particularly at low stellar masses. There is a relative dearth of low mass satellites near group centers; this could be a hint of satellite depletion due to mergers, but challenges in measuring photometry of faint objects near massive extended central galaxies could be a contributing factor so further investigation is needed. Similar evidence of mass segregation and the influence of mass and environment on star formation has been seen in groups and clusters out to $z \sim 1$ (Muzzin et al. 2012; Presotto et al. 2012). Many of these trends can be seen across the entire redshift range studied here, indicating that both stellar mass and halo environment play a role in determining galaxy properties at least since $z = 1$. Sample variance due to the finite survey volume does affect our ability to measure absolute redshift trends as the number densities vary significantly due to large-scale structures (particularly evident at $z = 0.3 - 0.4$), but the relative fractions of different populations should be less affected.

The central panel of Figure 1 shows a few examples of the three morphological classifications from ZEST, chosen randomly to span the range of colors seen from redshifts $z = 0.4 - 0.6$ and with $\log(M_*/M_\odot) > 10$. While these classifications do not always agree with one’s visual impression, there are clear differences in structural parameters among the classes, and correlations between these automated measurements and a galaxy’s position in a group can provide an interesting test of the dependence of morphology on environment. We emphasize

that the ZEST morphologies are correlated with, but not identical to, traditional visual classification of ellipticals and spirals. We compare results from multiple morphological indicators in Section 3.3.

3.1. Radial Trends: Blue Late Disks into Red Bulge+disks

We can quantify some of the trends from Figure 1 by measuring the fraction of galaxies of a given color and morphology as a function of stellar mass, group-centric distance, and redshift. Figure 2 shows the fraction of galaxies in each of the six combinations of color and morphology categories described in Section 2.2. For example, the cyan triangles represent the fraction of galaxies in the stellar mass and redshift range shown that are both blue and have late disk morphology. This population makes up the majority among field galaxies (shown at $R > R_{200c}$) but its fraction declines among satellites, contributing less than 20% of the satellite population at $R < R_{200c}/3$. Meanwhile, the proportion of red bulge+disk galaxies rises from 7% in the field to 40% among satellites in the inner radial bin.

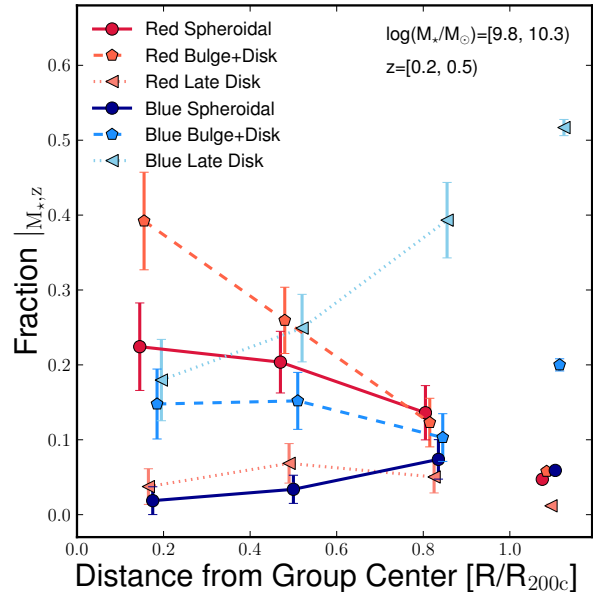


FIG. 2.— Color and morphological fractions as a function of group-centric distance. These fractions are calculated for satellites in three equally-spaced bins out to R_{200c} after applying contamination corrections. The field population is plotted to the right. Points are assigned small horizontal offsets for clarity. Error bars are the 1σ standard deviation of 500 bootstrap samples. There is a clear transition from blue late disks dominating among field galaxies and outer satellites to red bulge+disks among inner satellites.

Figure 2 highlights the most significant environmental trends in our sample by focusing on low mass, low redshift galaxies. We repeat the exercise in Figure 3 with higher mass and redshift bins to study how these trends vary. The broad picture is similar; blue late disks dominate in the field while the red bulge+disk population becomes more prominent toward group centers. Among low mass galaxies at $z > 0.5$, the blue late disks dominate everywhere, while more massive galaxies at lower

redshift have a substantial population of red spheroidals. Red late disks and blue spheroidals do not make up a large portion of galaxies at any mass or redshift studied. The red fraction can be determined from these plots by summing the three red lines, and similarly the spheroidal fraction is the sum of the solid lines with circular markers. The red fraction rises toward group centers for low mass galaxies, but is relatively flat among massive galaxies. We note that the abscissa for these plots is the projected group-centric distance, and that the true radial trends measured in spherical shells are likely more significant than observed.

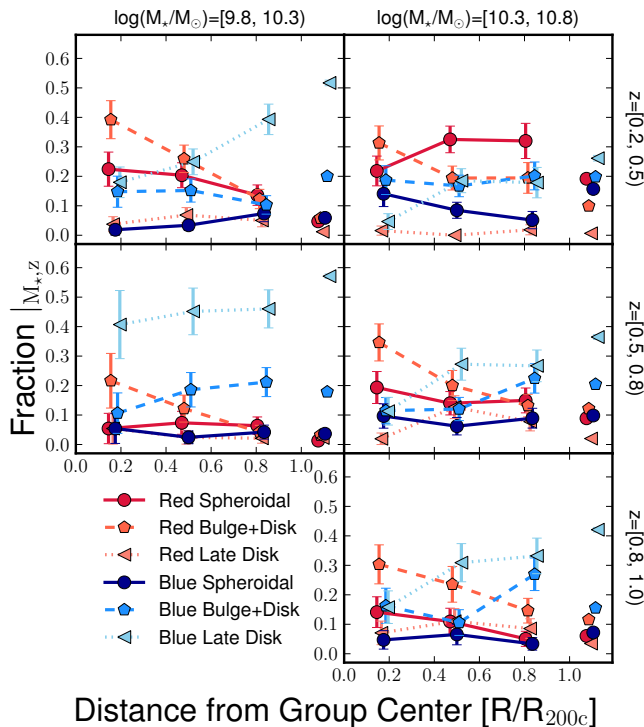


FIG. 3.— Color and morphological fractions of group members as a function of distance from the group center, for different bins of stellar mass (columns) and redshift (rows). Line styles and error bars are as defined in Figure 2. Figure 2 is repeated in the top left panel, for comparison with weakening environmental trends at higher mass and redshift.

3.2. Redshift Trends

Since satellites tend to fall toward halo centers, group-centric distance is related to the timescale that galaxies have been inside the group. The range of redshifts sampled with this data set provides another measure of time to study evolution. Figure 4 is a transpose of Figure 3 to show the redshift trends in the distribution of colors and morphologies. Again, there is a decline in blue late disks among low-mass satellites near the centers of groups, now compensated by a rise in both red spheroidals and red bulge+disks. This trend weakens away from group centers and at higher masses.

3.3. Checks for Systematics

3.3.1. Environment

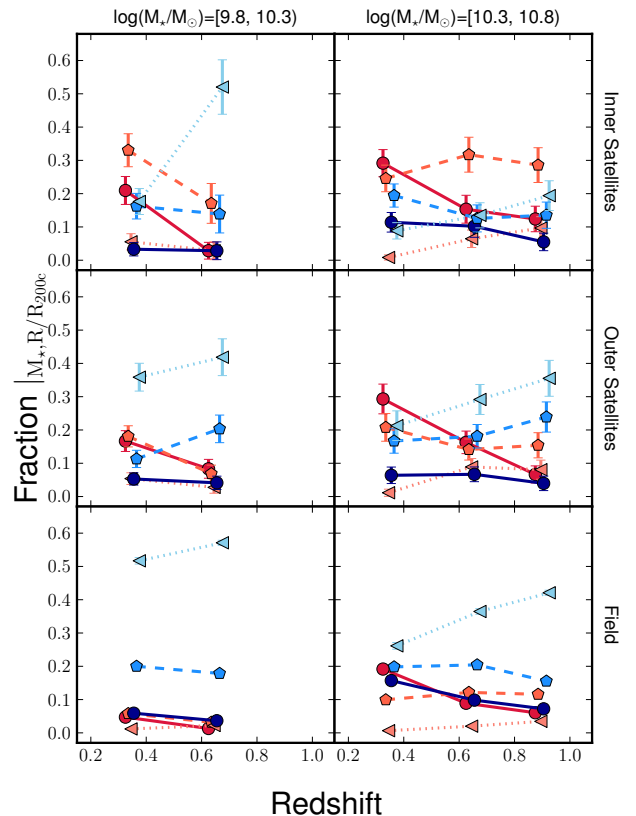


FIG. 4.— Color and morphological fractions as a function of redshift, for different bins of stellar mass (columns) and environment (rows). Inner and outer satellites are separated at a projected group-centric distance of $0.5R_{200c}$. Line styles and error bars are as defined in Figure 2.

There are several possible biases or other effects in the data to consider in order to ensure the robustness of these results. First, we revisit the contamination of our satellite sample due to interloping field galaxies, discussed in Section 2.1. In Figures 2, 3, and 4 we have plotted values of population fractions for satellites corrected for contamination estimated from mock catalogs. Contamination corrections are always smaller than the statistical error bars estimated via bootstrapping, except for low mass blue disk galaxies where it is 10% greater than the error because the field population is so large. Though the sample of satellites near R_{200c} is significantly contaminated by field galaxies, the corrections to the relative fractions of each galaxy type are small because the field populations are not markedly different from the outer satellites.

3.3.2. Color Distribution

When classifying galaxies by their spectral energy distributions (SEDs), our primary aim is to distinguish star-forming galaxies from those that are quenched. Though traditional indicators from emission lines or spectral breaks are not directly available from photometry, the 31-band SEDs used here provide a wealth of information about spectral types, including an estimate of dust extinction that separates star-forming galaxies that appear red due to dust from those that are truly passive. The

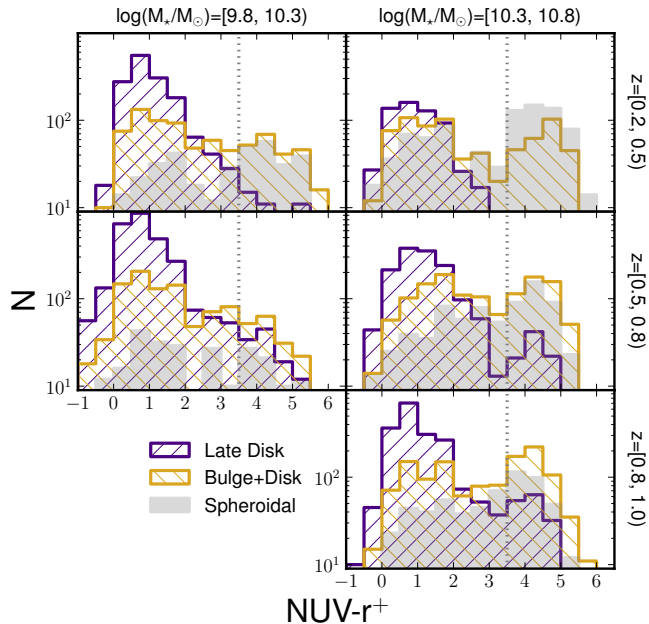


FIG. 5.— Distribution of rest-frame, extinction-corrected, template colors by morphological type. Galaxies from all environments are included. Vertical dotted lines show the cut used to segregate red and blue galaxies.

template-based, extinction-corrected ($\text{NUV} - r^+$) colors used in this paper generally have a bimodal distribution with the color cut from Section 2.2 falling on the red end of the “green valley.” The color distributions for different morphological types are shown in Figure 5. Shifting the cut slightly in either direction shifts the amplitude of the red fraction in Figures 2, 3, and 4 up or down, but the trends with group-centric distance and redshift do not vary significantly. We have tested an alternative “red sequence” selection suggested by Ilbert et al. (2010), $\text{NUV} - r^+ > 0.5 \log(M_*/M_\odot) - 0.8z - 0.5$, using rest-frame absolute magnitudes but applying no extinction correction. The transformation of blue late disks into red bulge+disks among low mass satellites is still evident. Similarly, applying the two-color cut in the $\text{NUV} - r^+$, $r^+ - J$ plane used by Bundy et al. (2010) does not qualitatively change our results.

3.3.3. Morphologies

Morphological classification is a challenging problem and significant scatter exists between the types assigned to galaxies in both visual and automated analyses. In general, visual analyses emphasize the presence or absence of spiral features, categorizing objects as spirals or ellipticals, often with an intermediate class of S0s grouped with ellipticals. Automated analyses measure structural parameters such as concentration and asymmetry which are then generally tied to a training set of visual classifications. The correlation between the properties measured is imperfect, so we test the impact on our results of using a variety of automated morphological classifications, all based on the ACS F814W imaging. The alternative classifications come from Tasca et al. (2009), which presented three separate techniques.

The differences between the results of each catalog and those from the ZEST classification used in this paper are

driven by how bulge+disk galaxies are classified, since the other catalogs do not split the spiral/disk category into multiple bins as ZEST does. For instance, among the 237 satellites used for Figure 2, the ZEST classifications are 22% spheroidal, 36% bulge+disk, 37% late disk, and 5% irregular or unclassified. The three separate classifications for these galaxies from Tasca et al. (2009) vary between 39 – 59% E/S0s and 59 – 40% spirals. When bulge+disk galaxies are mostly classified as E/S0s, the spheroidal populations (both blue and red) in Figures 3 and 4 are significantly elevated but show similar trends with group-centric distance and redshift. In the opposite case where bulge+disk galaxies are mostly treated as disks, the spheroidal fraction is essentially unchanged. While the dominant population in each panel of Figure 3 and 4 can change depending on which category the intermediate bulge+disk galaxies fall into, the radial trend in low mass satellites is unchanged; the blue late type fraction declines toward group centers and is compensated with a rise in red early types. The redshift trend for this transition is strongest for low mass satellites near group centers and weakens toward larger radii and stellar masses. Though the scatter between morphological classifications signals that our results should be interpreted and compared to others with caution, the significant trends with group-centric distance and redshift for the intermediate bulge+disk galaxies suggests that the ZEST classification has identified a population in transition.

3.3.4. A Population of Blue Spheroidals

While the tests described above suggest that our measures of environment, color, and morphology are robust, we do note a puzzling population of massive blue spheroidals that can be seen most clearly in the bottom right panel of Figure 4 as well as the right column of Figure 5. Those plots suggest that half of all spheroidals in that stellar mass range are blue, exceeding measurements in other studies (e.g. Kaviraj et al. 2007, 2008; Bamford et al. 2009; Schawinski et al. 2009; Ilbert et al. 2010), but see also Cross et al. (2004) who found a large fraction of blue ellipticals in a luminosity-selected sample at moderate redshift. We see a similarly large blue fraction among spheroidals at higher masses ($\log(M_*/M_\odot) > 10.8$, not plotted) where spheroidals make up a higher proportion of all galaxies, and most prominently at low redshift ($z < 0.5$). Visual inspection of the ACS images of these galaxies suggest that 30–40% show spiral or irregular features, although the structural parameters measured by the automated classifiers are all consistent with the red spheroidal population. We have also investigated the UV-optical and optical-IR colors of these massive blue spheroidals prior to template fitting, in addition to optical spectra for 30 of these objects described in George et al. (2011). These data suggest that blue spheroidals are not typical star-forming galaxies but may have a small amount of recent star formation to which rest-frame UV measurements are particularly sensitive (e.g. Kaviraj et al. 2007, 2008). Another possible explanation is that there are unusual stellar populations that are not represented in the template fits used to derive our $(\text{NUV} - r^+)$ colors (see e.g. Smith et al. 2012, for a discussion of galaxy properties contributing to the “UV upturn”). While this population is interesting in

its own right, it is most prominent at high stellar masses and does not show a strong dependence on environment, so we do not consider it further here.

4. DISCUSSION AND CONCLUSIONS

Our results indicate a complex relationship between color, morphology, stellar mass, and group-centric distance. Trends in color and morphology are distinct, and the use of a single property as proxy for galaxy type does not capture the whole picture. The most interesting trend seen is the shift in dominance among the low mass population from blue late disk galaxies in the outskirts to red bulge+disk types in group interiors. If part of one population was merely disappearing from the sample, either due to changes in mass or merging with other galaxies, then the other populations would all be expected to grow by an equal factor. The fact that the decline in one population is roughly balanced by the rise of a single other population suggests a transformation process. We now discuss these results in the context of past analyses, the physical implications of the present work, and future avenues to clarify the role of environment in galaxy evolution.

4.1. Connection to Previous Observations

There is a long history of research into the covariance between the stellar masses, colors, morphologies, and environments of galaxies and its evolution with time. After controlling for differences in stellar mass or luminosity, numerous studies at low redshift have found that color is more strongly correlated with environment than morphology (e.g., Kauffmann et al. 2004; Blanton et al. 2005; Christlein & Zabludoff 2005; van den Bosch et al. 2008; Bamford et al. 2009; Skibba et al. 2009; Weinmann et al. 2009). The implication of these studies is that the well-known correlation between morphology and environment is secondary to correlations between morphology and stellar mass or color, with the latter properties more physically linked to environment. Still, some of these studies find residual correlations between morphology and environment after controlling for color and stellar mass or luminosity, particularly at low masses and among late to intermediate morphologies (Blanton et al. 2005; Weinmann et al. 2009; Skibba et al. 2012).

Moving from large low-redshift studies to moderate redshifts ($z \sim 0.4$), Balogh et al. (2009) and McGee et al. (2011) have shown that groups still host a higher fraction of red galaxies than the field, while Wilman et al. (2009) found an elevated S0 fraction in groups with a mildly significant rise with group-centric distance. This radial trend in morphology is the opposite of that seen in Figure 3 but may be due to a smaller sample size or the use of luminosity-weighted centroids, which have been shown to be a poorer tracer of halo centers measured by weak lensing when compared with the most massive galaxy used in this catalog (George et al. 2012).

Environmental trends at fixed stellar mass have been seen to weaken at higher redshift (e.g., Poggianti et al. 2008; Tasca et al. 2009; Cucciati et al. 2010; Iovino et al. 2010; Kovač et al. 2010), though recent analyses have shown clear differences between the fraction of star-forming galaxies across environments over a range of stellar masses at least up to $z \sim 1$ (Cooper et al. 2010; Peng et al. 2010; George et al. 2011; Knobel et al.

2012). Tasca et al. (2009) and Kovač et al. (2010) have compared the dependence of colors and morphologies on local density and in groups in the COSMOS field, finding a stronger effect on color than on morphology, similar to the low redshift results and suggesting a longer timescale for structural transformations than for quenching star-formation. Muzzin et al. (2012) and Presotto et al. (2012) have also shown that the quenched fraction among satellites depends significantly on group-centric distance at these redshifts.

The results presented here extend this work to include radial trends in colors and morphologies from $z = 0.2 - 1$. Our X-ray group catalog gives a large, clean, and fairly representative selection of $10^{13} - 10^{14} M_{\odot}$ halos (Finoguenov et al. 2010), and has been well-calibrated based on its weak lensing signal (Leauthaud et al. 2010; George et al. 2012). We detect significant trends in both color and morphology with group-centric distance. Some previous studies measured weak or insignificant gradients in morphology by using a simple dichotomy of spirals and ellipticals, and we can reproduce these results when using a coarse morphological binning (see discussion in Section 3.3.3). But in contrast to those results, we see clear morphological gradients at fixed stellar mass and color once the morphological classification considers differences in the bulge content of disk galaxies.

The importance of this intermediate morphology between pure disks and spheroidals has been noted before in the context of S0 galaxies which have been known to dominate the evolution in the morphology-density relation (Dressler et al. 1997; Postman et al. 2005; Smith et al. 2005; Boselli et al. 2006; Moran et al. 2007; Oesch et al. 2010; Lackner & Gunn 2013). Smith et al. (2005) also showed that morphological evolution occurs later in less dense regions than in the densest regions associated with clusters, with little evolution at intermediate densities from $z = 1$ to 0.5 followed by an increase in early types at lower redshift. There is a significant overlap between the intermediate bulge+disk population in our analysis and visually classified S0 galaxies although these bulge+disk galaxies are often classified slightly later along the Hubble sequence (Scarlata et al. 2007). Our results in Figure 4 broadly corroborate those of Smith et al. (2005) and add that color and stellar mass are also important dimensions when studying these trends.

4.2. Implications for Physical Mechanisms of Galaxy Transformation

The radial gradients and redshift trends measured in Section 3 suggest a transformation among low mass satellites from blue late disks into red bulge+disks and spheroidals. The mechanism for this transformation must affect both color and morphology, or more physically, the star formation rate and stellar kinematics. Some processes (see e.g. Boselli & Gavazzi 2006, for a review) halt star formation without significantly altering stellar structure, such as gas removal via ram pressure stripping or weak tidal interactions, suppression of gas accretion within dense shock-heated environments, or quasar feedback. On the other hand, galaxy mergers and strong tidal interactions can affect both the distribution of gas needed to form stars as well as the stellar morphology. A third possibility is that color and morphology

changes are physically coupled; bulge growth could stabilize a galaxy against disk fragmentation and suppress star formation (Martig et al. 2009), or gas loss may leave a disk unable to dissipate energy from tidal interactions or may drive instabilities leading to bulge growth. Yet another scenario is that a bulge only appears more prominent after a galaxy is quenched because the previously star-forming disk has faded.

We can test these models by studying the morphological dependence on environment among quenched galaxies. Mechanisms like gas stripping or disk fading that do not directly affect morphology should produce a higher fraction of quenched galaxies in dense environments, but among quenched galaxies the morphological distribution should be constant across environments. On the other hand, if quenched galaxies in dense environments have more bulge-dominated morphologies than quenched field galaxies, it would suggest that mergers or strong tidal interactions altering the structure of galaxies occur in addition to, or in conjunction with, the suppression of star formation. The results of this test are plotted in Figure 6, where we show the fractions of red galaxies that are early and late type as a function of environment. We have used a broad redshift range and combined the spheroidal and bulge+disk categories to reduce statistical errors for this smaller population of red galaxies. Figure 6 demonstrates that quenched satellites, particularly those in the inner regions of groups, are more likely to be bulge-dominated than their field counterparts.

We interpret this to mean that some physical process in dense environments is driving bulge growth. Though some field studies (Bundy et al. 2010; Masters et al. 2010) have already noted a tendency of passive disks to be more concentrated than star-forming disks, we find that the morphological evolution of quenched galaxies is even stronger in groups. Our result is consistent with previous arguments favoring bulge growth over disk fading based on the higher typical luminosities of galaxies with intermediate morphologies compared to late types (Christlein & Zabludoff 2004; Burstein et al. 2005). The data presented here show that even at fixed mass there must be bulge enhancement that accompanies quenching in groups.

The results of Figure 3 suggest that the timescale for the morphological transition from late disk to bulge+disk must be comparable to the timescale for quenching in order to turn blue late disks directly into red bulge+disk galaxies. For example, if quenching occurred via gas stripping or removal at a rate faster than any structural changes, we would expect to see blue late disks turning into red late disks. Instead we observe a growth in red galaxies with earlier morphologies whenever blue late disks decline. The fraction of blue late disks plummets by more than a factor of two in ~ 2 Gyr among inner satellites (top left panel of Figure 4), while the fraction of red late disks is nearly constant and the fraction of red bulge+disks grows. Similarly, we do not detect a large population of blue bulge+disk galaxies which might be expected if bulge growth happened faster than quenching. These observations suggest that some morphological evolution occurs on a similar timescale as quenching.

At the same time, the morphological transformation observed at low stellar masses has not fully turned many disks into spheroidals. The bulge+disk galaxies are still

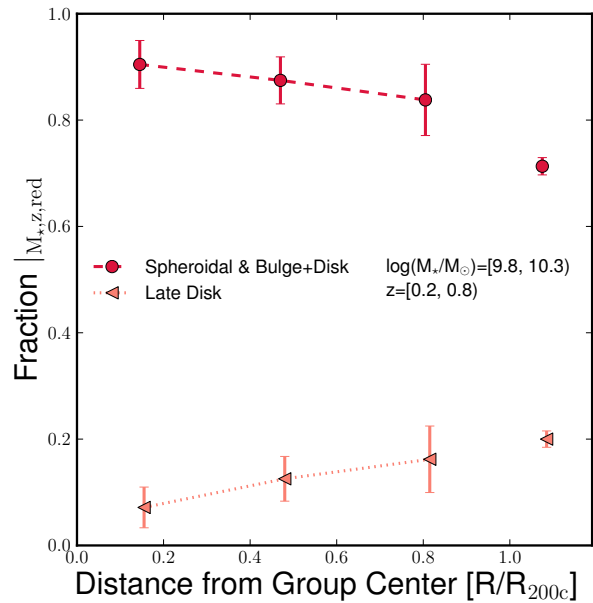


FIG. 6.— Morphological fractions *among red galaxies* as a function of distance from the group center. The small but significant excess in early-type morphologies among inner satellites relative to field galaxies suggests that mergers or tidal interactions cause more significant bulge growth among satellites.

categorized as disks in the top level ZEST classification. This echoes earlier results finding a buildup of S0s in clusters but weaker evolution in the relative abundance of ellipticals (e.g., Dressler et al. 1997). Though the fraction of red spheroidals does not correlate significantly with group-centric distance (Figure 3), it does grow globally with time (Figure 4). This may indicate that different processes are responsible for producing bulge+disks and spheroidals.

The discreteness of morphological classification makes detailed comparison of transformations in morphology and color somewhat difficult, but the structural evolution appears to contrast with that in color, where a clear bimodality separates red and blue states and the relatively low intermediate population suggests a fast quenching timescale once it begins (e.g., Wetzel et al. 2012a, though see Balogh et al. 2011). One could test the hypothesis that galaxies pass through an intermediate state between blue late disk and red bulge+disk by measuring the time since quenching based on the SEDs of galaxies in these intermediate states. Is there a difference in the mean color of blue bulge+disks and blue late disks, or between red bulge+disks and red late disks? Figure 5 does not show conclusive differences in the colors of these populations, and the satellite sample size is too small to constrain differences in the distribution of colors within the red and blue populations. More detailed analysis with spectroscopic data could better constrain such evolutionary models.

The group environment can play an important role in building up the well-studied color-morphology-density relations in nearby clusters. A group of mass $10^{13.5} M_{\odot}$ at $z = 1$ should grow through mergers by an average of 0.3 dex to $z = 0$ (Fakhouri et al. 2010), so some of our high redshift groups will be the progenitors of massive

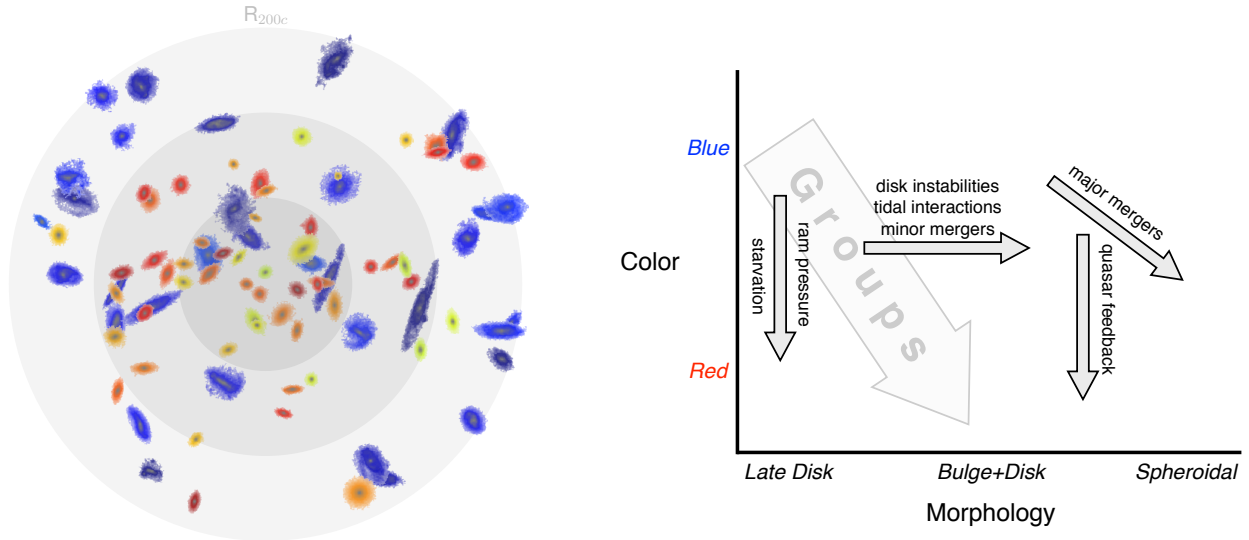


FIG. 7.— Illustrations of our main results and interpretation. Left panel shows the projected positions of satellites in an ensemble group with the same stellar mass and redshift range as Figure 2 with only the blue late disks (which dominate the outskirts) and red bulge+disks (which dominate the interior) displayed. The schematic diagram at right shows the effects of various physical mechanisms on color and morphology; the large arrow indicates the observed transformation from blue late disks to red bulge+disks, suggesting a combination of processes.

clusters and others may accrete onto them. For comparison, a typical star-forming galaxy should grow by 0.2 dex in stellar mass between each of our three redshift bins and by 0.7 dex from $z = 1$ to 0 (Elbaz et al. 2011). Wetzel et al. (2012b) show that the dominant population of satellites in the most massive halos at $z = 0$ were already satellites in groups when accreted. Our results demonstrate that both the color and morphology of these satellites are influenced in the group environment, showing the importance of “preprocessing” of galaxies prior to entering massive clusters. The bulge+disk population we see here is not quite as morphologically evolved as the growing S0 population seen at low redshift and in massive clusters, but likely precedes it.

We summarize our main results and interpretation in Figure 7. The left panel shows the positions of satellites for a stacked group and highlights the trend in Figure 2 with blue late disks dominating the outskirts and red bulge+disk galaxies making up most of the inner satellite population. This combination of color and morphology transformations suggests some combination of gas removal and bulge growth, shown in the right panel. While the diagram is a simplification of a wide variety of model predictions, the primary point is that *both* color and morphology are affected in group satellites, so physical mechanisms that explain environmental correlations should reflect this.

4.3. Future Prospects

While these measurements add insight to the transformation of galaxy properties, much work remains to be done to constrain the variety of physical mechanisms that may be responsible. A cleaner bulge-disk decomposition would be useful to track the growth of bulges and the importance of disk fading (e.g., Lackner & Gunn 2012, 2013). Incorporating the physical sizes of each compo-

nent would also help to link these transformations with the significant growth seen in early types since $z \sim 2$ (e.g., Bruce et al. 2012). With deep high-resolution imaging from *HST*, the CANDELS survey (Grogin et al. 2011; Koekemoer et al. 2011) is pushing these studies to higher redshift and should also allow bulge-disk decomposition to be studied at multiple wavelengths, identifying when and where star formation is happening or stopping. Alternatively, visual classifications from an ongoing Galaxy Zoo project in the CANDELS fields will track the evolution of spiral features and bars which are challenging for automated techniques. Impending wide field imaging surveys will add greatly to the statistics of these analyses.

Different measures of environment may also help disentangle the relevant physical mechanisms. While we have argued in favor of halo-based indicators (see George et al. 2011 for a discussion), the local galaxy density *within a halo*, in addition to group-centric distance, may shed light on galaxy-galaxy interactions and infalling substructure (e.g., Blanton & Berlind 2007; Cibinel et al. 2012; Woo et al. 2012). However, this indicator is a noisy quantity affected by shot noise, redshift errors, and peculiar velocities, likely requiring deep and complete spectroscopic data for clean results. Larger surveys will also enable a wider range of halo masses to be probed at higher redshift. Comparison of different halo mass proxies can provide a test of environmental mechanisms, for example if X-ray bright groups are more efficient at ram pressure stripping satellites than groups with less hot gas.

These studies can also be extended to the interplay of environmental mechanisms with non-stellar components of galaxies, namely the gas content and central black holes in galaxies. Current and planned radio arrays will extend the study of neutral and molecular gas beyond the local Universe allowing a clearer picture of how star formation is fed and quenched. And the growth of bulges

seen in this paper should be connected with accretion onto the central black hole in order to explain the tight correlation seen locally between these components.

Finally, while we have simply presented an empirical description of the data here, we can extend this work by modeling the evolution of color and morphology with environment. Peng et al. (2010) and Wetzel et al. (2012b) present simple empirical descriptions of the fraction of quenched galaxies as a function of stellar mass and environment. Incorporating morphologies into this framework will further illuminate the physical processes at work that build up the environmental correlations we observe.

We thank Andrew Wetzel, Frank van den Bosch, and Nic Ross for helpful discussions, and Claire Lackner

for constructive comments on a draft. MRG acknowledges support from the US Department of Energy's Office of High Energy Physics (DE-AC02-05CH11231) and a Graduate Research Fellowship from the US National Science Foundation. CPM is partially supported by a grant from the Simons Foundation (#224959). This work was also supported by World Premier International Research Center Initiative (WPI Initiative), MEXT, Japan. We gratefully acknowledge the contributions of the entire COSMOS collaboration. More information on the COSMOS survey is available at <http://cosmos.astro.caltech.edu>. This research has made use of the NASA/IPAC Infrared Science Archive, which is operated by the Jet Propulsion Laboratory, California Institute of Technology, under contract with the National Aeronautics and Space Administration.

REFERENCES

- Allevato, V., et al. 2012, *ApJ*, 758, 47
 Balogh, M. L., et al. 2009, *MNRAS*, 398, 754
 —. 2011, *MNRAS*, 412, 2303
 Bamford, S. P., et al. 2009, *MNRAS*, 393, 1324
 Blanton, M. R., & Berlind, A. A. 2007, *ApJ*, 664, 791
 Blanton, M. R., Eisenstein, D., Hogg, D. W., Schlegel, D. J., & Brinkmann, J. 2005, *ApJ*, 629, 143
 Blanton, M. R., & Moustakas, J. 2009, *ARA&A*, 47, 159
 Boselli, A., Boissier, S., Cortese, L., Gil de Paz, A., Seibert, M., Madore, B. F., Buat, V., & Martin, D. C. 2006, *ApJ*, 651, 811
 Boselli, A., & Gavazzi, G. 2006, *PASP*, 118, 517
 Bruce, V. A., et al. 2012, *ArXiv e-prints*
 Bruzual, G., & Charlot, S. 2003, *MNRAS*, 344, 1000
 Bundy, K., et al. 2010, *ApJ*, 719, 1969
 Burstein, D., Ho, L. C., Huchra, J. P., & Macri, L. M. 2005, *ApJ*, 621, 246
 Cassata, P., et al. 2005, *MNRAS*, 357, 903
 Chabrier, G. 2003, *PASP*, 115, 763
 Christlein, D., & Zabludoff, A. I. 2004, *ApJ*, 616, 192
 —. 2005, *ApJ*, 621, 201
 Cibinel, A., et al. 2012, *ArXiv e-prints*
 Cooper, M. C., et al. 2010, *MNRAS*, 409, 337
 Cross, N. J. G., et al. 2004, *AJ*, 128, 1990
 Cucciati, O., et al. 2010, *A&A*, 524, A2
 Dressler, A. 1980, *ApJ*, 236, 351
 Dressler, A., et al. 1997, *ApJ*, 490, 577
 Elbaz, D., et al. 2011, *A&A*, 533, A119
 Fakhouri, O., Ma, C.-P., & Boylan-Kolchin, M. 2010, *MNRAS*, 406, 2267
 Finoguenov, A., et al. 2007, *ApJS*, 172, 182
 —. 2010, *MNRAS*, 403, 2063
 Ford, J., et al. 2012, *ApJ*, 754, 143
 George, M. R., et al. 2011, *ApJ*, 742, 125
 —. 2012, *ApJ*, 757, 2
 Grogin, N. A., et al. 2011, *ApJS*, 197, 35
 Ilbert, O., et al. 2009, *ApJ*, 690, 1236
 —. 2010, *ApJ*, 709, 644
 Iovino, A., et al. 2010, *A&A*, 509, A40
 Kauffmann, G., White, S. D. M., Heckman, T. M., Ménard, B., Brinchmann, J., Charlot, S., Tremonti, C., & Brinkmann, J. 2004, *MNRAS*, 353, 713
 Kaviraj, S., et al. 2007, *ApJS*, 173, 619
 —. 2008, *MNRAS*, 388, 67
 Knobel, C., et al. 2012, *ArXiv e-prints*
 Koekemoer, A. M., et al. 2007, *ApJS*, 172, 196
 —. 2011, *ApJS*, 197, 36
 Kovač, K., et al. 2010, *ApJ*, 718, 86
 Lackner, C. N., & Gunn, J. E. 2012, *MNRAS*, 421, 2277
 —. 2013, *MNRAS*, 428, 2141
 Leauthaud, A., et al. 2010, *ApJ*, 709, 97
 —. 2012, *ApJ*, 744, 159
 Lotz, J. M., Primack, J., & Madau, P. 2004, *AJ*, 128, 163
 Martig, M., Bournaud, F., Teyssier, R., & Dekel, A. 2009, *ApJ*, 707, 250
 Masters, K. L., et al. 2010, *MNRAS*, 405, 783
 McGee, S. L., Balogh, M. L., Wilman, D. J., Bower, R. G., Mulchaey, J. S., Parker, L. C., & Oemler, A. 2011, *MNRAS*, 413, 996
 Moran, S. M., Ellis, R. S., Treu, T., Smith, G. P., Rich, R. M., & Smail, I. 2007, *ApJ*, 671, 1503
 Muzzin, A., et al. 2012, *ApJ*, 746, 188
 Navarro, J. F., Frenk, C. S., & White, S. D. M. 1996, *ApJ*, 462, 563
 Oesch, P. A., et al. 2010, *ApJ*, 714, L47
 Peng, Y.-j., Lilly, S. J., Renzini, A., & Carollo, M. 2012, *ApJ*, 757, 4
 Peng, Y.-j., et al. 2010, *ApJ*, 721, 193
 Poggianti, B. M., et al. 2008, *ApJ*, 684, 888
 Postman, M., et al. 2005, *ApJ*, 623, 721
 Presotto, V., et al. 2012, *A&A*, 539, A55
 Scarlata, C., et al. 2007, *ApJS*, 172, 406
 Schawinski, K., et al. 2009, *MNRAS*, 396, 818
 Schmidt, F., Leauthaud, A., Massey, R., Rhodes, J., George, M. R., Koekemoer, A. M., Finoguenov, A., & Tanaka, M. 2012, *ApJ*, 744, L22
 Scoville, N., et al. 2007, *ApJS*, 172, 1
 Skibba, R. A., et al. 2009, *MNRAS*, 399, 966
 —. 2012, *MNRAS*, 423, 1485
 Smith, G. P., Treu, T., Ellis, R. S., Moran, S. M., & Dressler, A. 2005, *ApJ*, 620, 78
 Smith, R. J., Lucey, J. R., & Carter, D. 2012, *MNRAS*, 421, 2982
 Tasca, L. A. M., et al. 2009, *A&A*, 503, 379
 Tinker, J. L., George, M. R., Leauthaud, A., Bundy, K., Finoguenov, A., Massey, R., Rhodes, J., & Wechsler, R. H. 2012, *ApJ*, 755, L5
 van den Bosch, F. C., Aquino, D., Yang, X., Mo, H. J., Pasquali, A., McIntosh, D. H., Weinmann, S. M., & Kang, X. 2008, *MNRAS*, 387, 79
 Weinmann, S. M., Kauffmann, G., van den Bosch, F. C., Pasquali, A., McIntosh, D. H., Mo, H., Yang, X., & Guo, Y. 2009, *MNRAS*, 394, 1213
 Weinmann, S. M., van den Bosch, F. C., Yang, X., & Mo, H. J. 2006, *MNRAS*, 366, 2
 Wetzel, A. R., Tinker, J. L., & Conroy, C. 2012a, *MNRAS*, 424, 232
 Wetzel, A. R., Tinker, J. L., Conroy, C., & van den Bosch, F. C. 2012b, *ArXiv e-prints*
 Wilman, D. J., Oemler, Jr., A., Mulchaey, J. S., McGee, S. L., Balogh, M. L., & Bower, R. G. 2009, *ApJ*, 692, 298
 Woo, J., et al. 2012, *ArXiv e-prints*